Coherent Raman Spectra of the ν_1 Mode of Carbon Suboxide

Tony Masiello, Andrea J. Voorhees, Mark J. Abel, and Joseph W. Nibler*

Department of Chemistry, Oregon State University, Corvallis, Oregon 97331-4003

Received: December 10, 2004; In Final Form: January 29, 2005

High-resolution (0.001 cm^{-1}) coherent anti-Stokes Raman spectroscopy (CARS) has been used to study the ν_1 symmetric CO stretching mode of the quasi-linear molecule carbon suboxide, C_3O_2. Q-branch transitions are seen that originate from the ground state and from thermally populated levels of the ν_7 CCC bending mode, which is of unusually low frequency. The intensity variation of the Q-branch features on cooling to about 120 K in a jet expansion requires the reversal of the order of assignment given in a previous Raman study at low resolution. The identification of the $\nu_1\ \Sigma_g^+ \leftarrow \Sigma_g^+$ transition from the ground state is confirmed by the absence of J_{odd} Q-branch lines in the resolved CARS spectrum. Analysis of this band in terms of a quasi-linear model gives a good fit to the observed transitions and leads to vibrational−rotational parameters (in cm^{-1}) of $\nu_1 = 2199.9773(12)$ and $(B' - B'') = -2.044(6) \times 10^{-4}$. Other transitions originating from higher ν_7 levels occur at only slightly lower wavenumber values and permit the calculation of the double minimum potential in the Q_7 bending coordinate. The results indicate that the ground-state barrier to linearity (21.5 cm^{-1}) increases by only 0.6 cm^{-1} when the CO symmetric stretch is excited.

Introduction

Carbon suboxide, C_3O_2, is an unusual molecule that has fascinated and puzzled spectroscopists for decades. First prepared by Diels and Wolf in 1906,[1] C_3O_2 is a colorless lachrymator with a boiling point of 7 °C. Though the least common of the simple carbon oxides, C_3O_2 is ubiquitous. It is believed to play a role in photochemical reactions in the atmospheres of Earth[2,3] and Venus[4,5] and to exist on the surface of the moons of Jupiter[6,7] and in Halley's comet.[8,9] At high gas pressures or in the liquid state, it readily undergoes polymerization to form a red solid film; Oyama[10] has suggested that the latter may even contribute to the red color of the Martian surface, where carbon suboxide is proposed as a photolytic reaction product of CO_2.

From structural and spectroscopic standpoints, carbon suboxide has long intrigued spectroscopists because of its floppy structure, as indicated by the ν_7 CCC bending frequency[11] of 18.26 cm^{-1}. To our knowledge, this is the lowest value observed for any "linear" molecule. In fact, calculations and experiments indicate that the equilibrium structure of C_3O_2 is bent and even slightly W-shaped, with recent ab initio calculations by Koput[12] yielding CCC and CCO angles of 152.0° and 176.5°, respectively. However, all calculations and experimental results indicate that the barrier to linearity is small (0−40 cm^{-1}), so the vibrationally averaged ground-state structure is linear. C_3O_2 is thus termed a "quasi-linear molecule", similar to the C_3 molecule, for which the bending mode is also quite low (63 cm^{-1}).[13]

The vibrational modes of carbon suboxide are shown in Figure 1. Because of the effective center of symmetry, the rule of mutual exclusion applies, with ν_1, ν_2, and ν_5 modes directly observable only by Raman methods,[14−16] while the other modes appear only in the IR, where they have been studied extensively.[11,16−23] In all cases, the spectra show added hot band structure arising from thermally populated levels of the ν_7 bending mode. Detailed analyses of the resultant spectra have

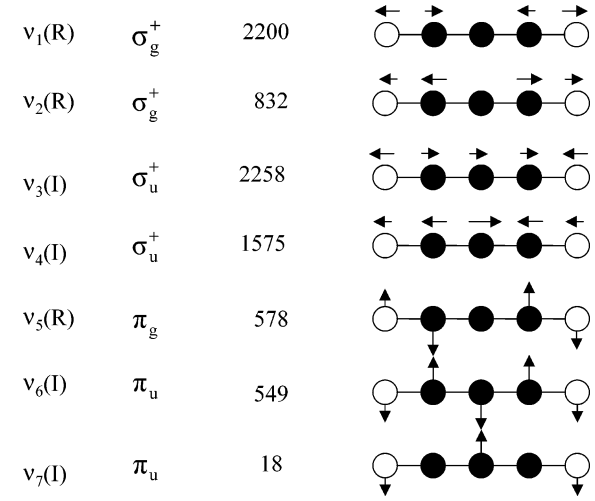

Figure 1. The vibrational modes of C_3O_2.

revealed the ν_7 level structure in the vibrational manifolds of the ν_2 through ν_6 fundamentals, as discussed by Fusina and Mills.[20] From the observed level spacings, quadratic and quartic parameters were deduced for a two-dimensional bending potential for each manifold. The results showed that the potential barrier and the pattern of levels are quite sensitive to excitation of a normal mode. For example, on excitation of the ν_2 symmetric CC stretch, the barrier drops to about zero from a value of 22 cm^{-1} in the ground state. However, antisymmetric excitation of the ν_4 CC stretch more than doubles the barrier, to 49.3 cm^{-1}, and the increase is even greater (65.3 cm^{-1}) when the ν_3 antisymmetric CO stretch is excited. Less dramatic are the effects of excitation in the ν_5 symmetric and ν_6 antisymmetric CCO bends, the barriers being 29.9 and 19.7 cm^{-1}, respectively.[21,22]

Although Raman spectra have been reported[14] for the ν_1 symmetric CO stretch, the effect of excitation of this mode on the ν_7 barrier has not been examined in detail and is perhaps

10.1021/jp044358j CCC: $30.25
Published on Web 03/19/2005

not obvious. By analogy with the barrier change seen on excitation of the CCC symmetric stretch, one might expect a decrease in the barrier when ν_1 is excited. However, it is also true that excitation of the antisymmetric CO stretch results in a large barrier increase. The most recent (1979) Raman data on ν_1 is of low resolution[14] (0.25 cm^{-1}) but does reveal some hot band structure that suggests that the barrier is quite similar to that in the ground state. Because CARS spectra can now be obtained with much greater sensitivity and resolution, it was felt that a reexamination of the ν_1 Q-branch structure might be worthwhile, and the results of this investigation are reported here.

Experimental Section

In these studies, C_3O_2 was prepared through dehydration of malonic acid by phosphorus pentoxide, P_2O_5, using the procedure of Maki et al.[23] The malonic acid, powdered P_2O_5, and sand (to increase the reaction surface area) were mixed together in a 1:10:2 ratio and then heated to 140 °C in an oil bath, while the vapors were collected in a liquid nitrogen cold trap. To reduce contamination from water, the sand was pre-roasted while being evacuated, and the chemicals were mixed together in a dry bag. The main products of the reaction were C_3O_2, acetic acid, and CO_2. The latter was removed by pumping on the trap at −110 °C, a temperature at which the vapor pressures of CO_2 and C_3O_2 are 33.3 and 0.2 Torr, respectively.[24,25] The C_3O_2 was separated from the acetic acid by warming the trap to −50 °C (vapor pressures of C_3O_2 and acetic acid are 45.8 and 0.1 Torr, respectively) and distilling the C_3O_2.

The CARS apparatus at Oregon State University used to obtain the high-resolution Raman spectra has been described previously.[26] This system is unusual for Raman spectroscopy in that the overall effective resolution capability has been shown to be very good, 0.001 cm^{-1}. The unique component of this system is a seeded, single-frequency Nd:YAG laser (Continuum, custom laser) that is frequency-doubled to deliver 45−50-ns pulses of 532-nm light at 20 Hz and 100 mJ/pulse. This long pulse, about 10 times that of most commercial lasers, gives the high spectral resolution of our system. The frequency of the Nd:YAG laser was locked to 18788.4624(15) cm^{-1} by adjusting the temperature controller on the seed laser (Lightwave model 122, 50 mW) and monitoring the output through a cell of iodine vapor such that the frequency of the green light corresponded to a position of 50% absorption intensity on the blue side of line no. 1111 of the iodine atlas.[27] Part of this green output is used to pump a pulse amplification chain for the tunable Stokes source that originates from a ring dye laser (Coherent, 699-29) pumped with 6 W from an argon ion laser (Coherent, Innova 200). Two portions of the 532-nm output were focused along with the amplified Stokes beam into the sample in a folded BOXCARS geometric arrangement. The signal was spatially and optically filtered before being detected by a Hamamatsu R955 photomultiplier and integrated by a Stanford Research signal averager (SR 250). A small portion of the light from the ring dye laser was sent through a cell of iodine vapor and recorded in order to calibrate the spectra using the iodine atlas lines.[27]

Because of its reactivity and tendency to polymerize, the sample was kept frozen at 77 K until use. All handling of C_3O_2 was done in glass vacuum manifolds and cells with Teflon stopcocks and connectors. Spectra were recorded of samples at 4 kPa (30 Torr) in glass cells and also in jet expansions in which Ar gas at about 0.5 atm was flowed through a C_3O_2 reservoir held at temperatures chosen to give a 50% mix. Because of the very limited amount of C_3O_2 available, the spectral scans in jets were taken rapidly, and it was not possible to be certain that the concentration was constant during all scans. Thus, although the wavenumber positions of features seen in the jet spectra were reproducible in the figures shown here, the relative intensities of the Q-branch features are less certain.

To minimize decomposition of the sample during the static scans, the power of the probe beams was kept to less than 2 mJ/pulse. Surprisingly, when the intensity of the beams was too great, scattering due to polymeric "dust" originated at the ends of the sample cell rather than at the center where the intensity of the focused beams was the greatest. This leads us to believe that the polymerization occurred because of heating on the window surface.

For the jet spectra, the sample cell was replaced with a vacuum chamber that was evacuated such that it maintained a pressure of less than 0.1 Torr throughout the measurements. The sample was introduced into the chamber through a jet nozzle whose pulse was temporally adjusted to match the timing of the pump and probe beams. The spectra were taken at a position early in the expansion (about one to two nozzle diameters), because the signal to noise was better there, and also, the warmer jet close to the nozzle made it possible to measure a number of the rotational lines in the vibrational Q-branches. The CARS signals in the jet were weak because of the low C_3O_2 concentration, so the power of the pump and Stokes beams were increased to around 13 and 3 mJ/pulse, respectively. At such power levels, we found in previous studies[28] that saturation and ac-Stark broadening effects limit the resolution to about 0.004 cm^{-1}. This is about twice the expected Doppler width but is sufficiently fine to resolve the individual Q-lines, as seen in the experimental spectra shown in the text.

Results and Discussion

CARS Spectra of C_3O_2. Figure 2 offers a comparison of the previous Raman spectrum and the CARS spectra obtained in this work. The top trace (a) shows a portion of the Raman spectrum recorded at 0.25 cm^{-1} resolution by Lolck and Brodersen,[14] and the dominant Q-branch is seen to consist of several unresolved features that they assigned to ν_7 hot bands according to the labeling shown at the top. An expanded view of this structure is seen in the higher-resolution CARS spectrum shown in the middle (b), and it is apparent that some of the Q_J line structure is discernible. However, because of the high line density and collisional broadening at the 30-Torr sample pressure, a detailed analysis was not possible. It was for this reason that CARS spectra were taken for C_3O_2 samples cooled by expansion in a jet, where it was hoped that collisional broadening would be reduced and vibrational and rotational cooling might simplify the spectra.

The effect of jet cooling shown in the CARS spectrum (c) of Figure 2 was quite surprising to us, because it showed a dramatic enhancement of the two higher-wavenumber Q-branches and a great reduction in intensity of the other branches seen in the room temperature scan. Clearly, the previous assignment of the Raman transition from the ground state to one of the latter is incorrect, and in fact, the data suggest a reversal of the order of assignment, as shown in the middle of the figure.

It is, of course, possible that either of the two main Q-branches seen in the jet spectra could be due to the $\Sigma-\Sigma$ transition from the ground state, but a closer look at the rotational structure of these is revealing. Figure 2c shows that the rotational lines in the highest-wavenumber branch are more clearly defined than is the case in the other Q-branch. This is

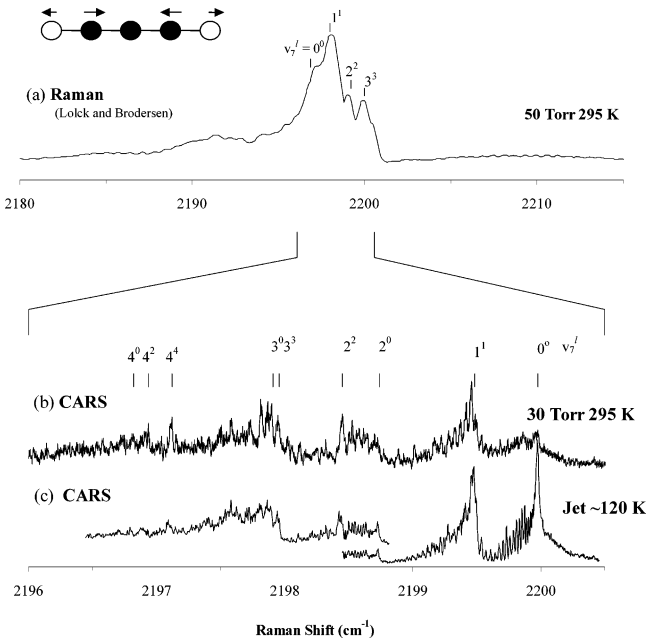

Figure 2. Raman and CARS spectra of C_3O_2. The Raman spectrum ((a), 0.25 cm^{-1} instrumental resolution, adapted from Figure 1 of ref 15) shows a dominant but unresolved Q-branch. The CARS spectrum (0.001 cm^{-1} instrumental resolution) taken at 295 K (b) reveals Q-branch features complicated by high line density and collisional broadening. The jet-cooled sample (c) clearly shows the $\nu_7{}^l = 0-3$ vibrational transitions. Note that the order of assignment in panel (b) is different than that given in panel (a).

expected for transitions from the ground Σ state, because J_{odd} levels, and hence J_{odd} Q-branch lines, will be missing because of nuclear spin constraints. (Both ^{12}C and ^{16}O atoms are bosons with nuclear spin of zero, so only nuclear spin functions that are symmetric to the exchange of identical particles are allowed.) However, for degenerate Π and Δ states, all lines are present, and the features are less resolved.

Modeling of Spectra. From the spectra, there can be no doubt that the highest-wavenumber Q-branch corresponds to transitions from $\nu_7{}^l = 0°$. These transitions are expected to fit the simple expression

$$Q_J = \nu_0 + (B' - B'')J(J+1) - (D' - D'')[J(J+1)]^2 \quad (1)$$

but this fitting requires assignment of J for each transition, a nontrivial task, because the transitions at low J are not resolved. The process required an initial guess for $B' - B''$, along with the reasonable assumption that the centrifugal distortion term $D' - D''$ could be neglected. We obtain one estimate of $B' - B''$ by assuming the same extension of the CO bond length ($\Delta r = 0.52$ pm) as is seen in exciting the CO diatomic molecule from $\nu = 0$ to $\nu = 1$. Assuming the CC distance is unchanged when CO is excited, this yields $B' - B'' = -0.00026$ cm^{-1}. A second estimate comes from Fusina and Mills,[20] who obtained $B' - B''$ as -0.00023 cm^{-1} from an anharmonic force field calculation. Finally, from a tentative assignment of some partially resolved S-branch Raman lines (seen in Figure 2a), Lolck and Brodersen[14] reported a value of $-0.00012(2)$ cm^{-1} for $B' - B''$. However, as mentioned already, their choice of band origin is incorrect, so this result for $B' - B''$ must also be in error. From a reanalysis of their S-branch lines using our revised band origin assignment, we get a larger value of $-0.00018(2)$ cm^{-1}.

From our higher-resolution Q-branch data, the best fit was obtained for the J assignment indicated in Figure 3 and in Table

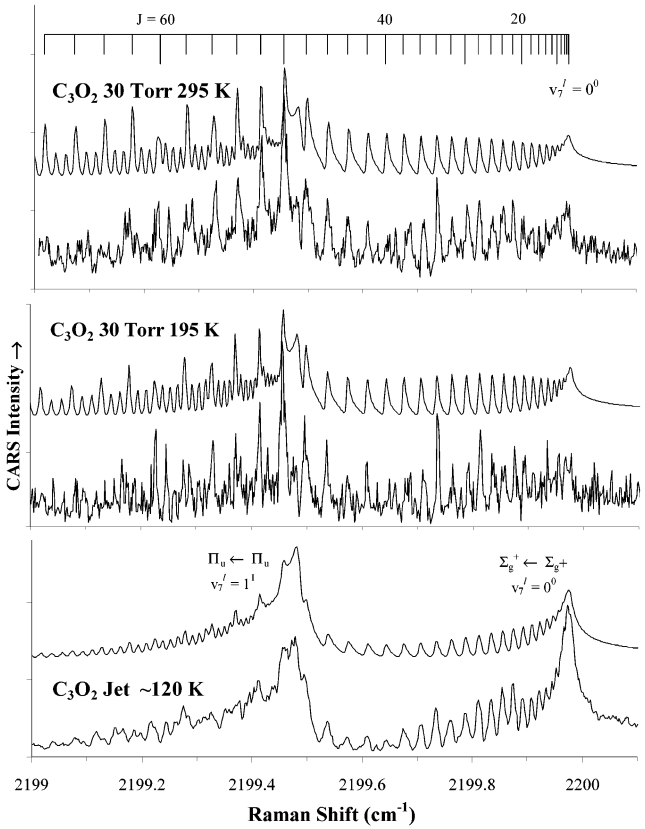

Figure 3. The vibrational−rotational modeling of the $\nu_7{}^l = 0^0$ and 1^1 Q-branches of C_3O_2. The predicted CARS spectrum using parameters given in the text is displayed above each experimental curve.

1. The resultant parameters for this assignment and cases where J is changed by ± 2 units are

$$J+2:\ \nu_0 = 2199.9905(21);\ B' - B'' = -0.0001941(10)$$

$$J:\ \nu_0 = 2199.9773(12);\ B' - B'' = -0.0002044(6)$$

$$J-2:\ \nu_0 = 2199.9643(18);\ B' - B'' = -0.0002159(11)$$

with uncertainties shown in parentheses here and elsewhere equal to two standard deviations. All the $B' - B''$ values above are in reasonable accord with the estimates given, but the J assignment choice is favored, because changes by ± 2 units give larger standard errors in the fit and also a visibly poorer reproduction of the CARS spectrum. However, the differences are small, so these alternative assignments cannot be completely eliminated. For J changes of ± 4 units or larger, the fits were clearly unacceptable.

There is one other complication to the fitting process that warrants mention. Because of interference effects by overlapping lines in CARS spectra, it is well-known that the peak maxima can be shifted a few thousandths of a wavenumber from the true transition frequencies.[29] To deduce these small corrections, an iterative fitting process was employed, with preliminary peak maxima from the CARS spectra first being used to generate by least squares a set of fitting parameters. These were used to calculate a set of transitions and intensities (assuming a Boltzmann rotational distribution) that were then used to simulate a CARS spectrum using procedures outlined in ref 29. The calculated shifts between the peak maxima and the actual input transition values were then applied to the experimental

TABLE 1: CARS Transitions and Vibrational−Rotational Parameters of C_3O_2

Q-Branch Lines (cm^{-1}) for the $\Sigma_g^+(0^0) \leftarrow \Sigma_g^+(0^0)$ Transition					
J	calcd	obsd − calcd	*J*	calcd	obsd − calcd
0	2199.9773				
2	2199.9760		32	2199.7614	−0.0004
4	2199.9732		34	2199.7340	0.0010
6	2199.9687		36	2199.7050	0.0034
8	2199.9626		38	2199.6743	0.0017
10	2199.9548		40	2199.6420	0.0001
12	2199.9454	−0.0011	42	2199.6081	−0.0016
14	2199.9343	−0.0009	44	2199.5725	−0.0026
16	2199.9217	−0.0011	46	2199.5353	−0.0026
18	2199.9074	−0.0002	48	2199.4965	−0.0025
20	2199.8914	0.0001	50	2199.4560	−0.0015
22	2199.8738	−0.0002	52	2199.4139	0.0001
24	2199.8546	0.0004	54	2199.3702	0.0013
26	2199.8338	0.0013	56	2199.3248	0.0041
28	2199.8113	0.0006	58	2199.2778	−0.0014
30	2199.7872	0.0020	60	2199.2291	0.0001

Parameters (in cm^{-1})

$\nu_7^{l\prime} \leftarrow \nu_7^{l\prime\prime}$	transition	ν_o obsd	ν_o diff. obsd	ν_o diff. calcd	$E'(\nu_7^l) - E'(0_7^0)^b$ obsd	$B' - B'' \times 10^4$ obsd
$0^0 \leftarrow 0^0$	$\Sigma_g^+ \leftarrow \Sigma_g^+$	2199.9773(12)[a]	(0)	(0)	0.00	−2.044(6)[a,c]
$1^1 \leftarrow 1^1$	$\Pi_u \leftarrow \Pi_u$	2199.484[2]	0.49	0.62	17.76	−2.064
$2^2 \leftarrow 2^2$	$\Delta_g \leftarrow \Delta_g$	2198.449[10]	1.53	1.31	44.58	−2.081
$2^0 \leftarrow 2^0$	$\Sigma_g^+ \leftarrow \Sigma_g^+$	2198.739[10]	1.24	1.24	59.46	−2.063
$3^3 \leftarrow 3^3$	$\Phi_u \leftarrow \Phi_u$	2197.959[10]	2.02	2.05	78.60	−2.097
$3^1 \leftarrow 3^1$	$\Pi_u \leftarrow \Pi_u$	2197.907[10]	2.07	2.08	95.15	−2.082
$4^4 \leftarrow 4^4$	$\Gamma_g \leftarrow \Gamma_g$	2197.12[?]	2.86	2.83	117.51	−2.111
$4^2 \leftarrow 4^2$	$\Delta_g \leftarrow \Delta_g$	2196.94[?]	3.04	2.93	134.22	−2.098
$4^0 \leftarrow 4^0$	$\Sigma_g^+ \leftarrow \Sigma_g^+$	2196.82[?]	3.16	2.95	141.14	−2.091

[a] Uncertainties in () are twice the standard error of the fit. Those in [ ] are estimates or are unknown. [b] Based on the $E''(\nu_7^l)$ values from ref 11. [c] $B' - B''$ values for the other transitions are this value scaled by the respective B'' values from ref 11.

maxima seen in the CARS spectra to obtain the experimental CARS transition frequencies. These corrected values were then used to deduce new fitting parameters, and the process was repeated to obtain slightly improved shift corrections. Convergence was rapid, and the corrections for each line, while small (−0.004 to +0.004 cm^{-1}), are significant at the fitted level. This process was done separately for spectra taken at different temperatures, and the resultant averaged experimental transition frequencies are shown in Table 1.

The simulations of the $\nu_7^l = 0^0\ \Sigma_g^+ \leftarrow \Sigma_g^+$ Q-branch shown in Figure 3 for the three temperatures are considered quite acceptable, given the high spectral congestion and noise in the spectra. For the jet spectra, the temperature was not well-determined, and lower values down to about 80 K also gave reasonable fits. Although some rotational structure was apparent for the other Q-branches, the lines were heavily overlapped, and no attempt was made to obtain $B' - B''$ for these bands. Instead, ΔB for these transitions was obtained from that for $\nu_7^l = 0^0$, scaled by the appropriate ground-state B values (viz., $\Delta B(\nu_7^l) = \Delta B(0^0)B''(\nu_7^l)/B''(0^0)$). The ν_0 band origins of the simulations were then adjusted to give the closest visual fit of the low *J*-band heads, and the resultant ν_0 values are listed in Table 1.

The assignments of the $\nu_7^l = 0^0$ and 1^1 Q-branches were certain from the intensity changes with temperature, and that for 2^0 was based on the more resolved *J* structure expected, and seen, for this $\Sigma_g^+ \leftarrow \Sigma_g^+$ band. For $\nu_7^l = 2^2$ and higher values, the assignments were based on ν_0 values predicted from a double minimum potential model described in the next section.

Double Minimum Potential Model. The model employed here is that used by Fusina and Mills[20] to describe the ν_7 bending potential in the ground state and its variation as other vibrational modes are excited. It assumes the anharmonic potential can be described by the function

$$V/hc = V_2\theta^2 + V_4\theta^4 = (V_2/m)Q_7^{\ 2} + (V_4/m^2)Q_7^{\ 4} \quad (2)$$

where θ is the angle of bend at the central carbon, Q_7 is the mass-weighted normal coordinate, and *m* is the effective mass, deduced from a normal coordinate calculation[20] to be 11.72 u Å^2. The ν_7 energy levels are then obtained as the eigenvalues of the Schrödinger equation for an isotropic two-dimensional harmonic oscillator, as detailed by Duckett et al.[30] We have reproduced this calculation using a simple Maple routine to diagonalize the appropriate matrix, taken to be of dimension 200 to ensure convergence of the lower levels. We obtain the same results reported by Fusina and Mills and have used this method to calculate the V_2 and V_4 potential parameters that apply when the ν_1 symmetric stretch is excited. These parameters were initially varied to give the best fit of our 0^0, 1^1, and 2^0 levels, and the results led to the assignment of higher v_7^l levels, producing the predicted Q-branch shifts shown in Table 1. The spectral simulations of these higher Q-branches are given in Figure 4. The comparison is considered acceptable, although the assignment of the $\nu_7 = 4$ bands should be considered tentative, because there appear to be other hot band features contributing to the spectra, possibly from excited ν_5 and ν_6 bending levels.

The potential constants deduced in this fashion are given in Table 2 for the ground state and for all the axial modes. Displays of these potentials, patterned after a similar figure in ref 20, are presented in Figure 5. It is seen that excitation of the ν_1 symmetric CO stretch has only a minor effect on the bending mode potential, the barrier height V_B increasing from 21.5 to 22.1 cm^{-1} and the value of θ at the energy minimum, θ_{min}, changing from 24.0° to 24.5°. This is perhaps not surprising,

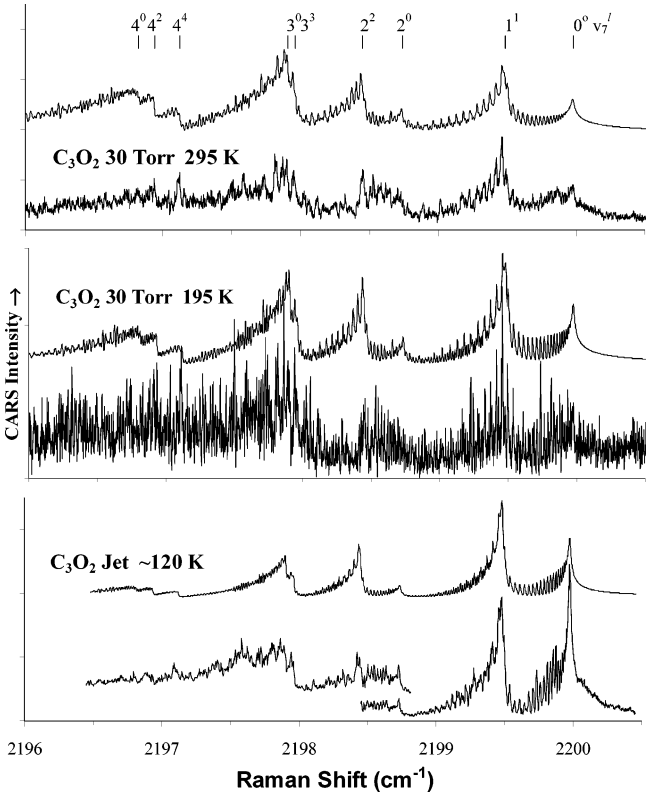

Figure 4. The vibrational−rotational modeling of the observed Q-branches of C_3O_2. The predicted CARS spectrum using parameters given in the text is displayed above each experimental curve.

TABLE 2: Parameters Defining the ν_7 Potential for Different Vibrational Manifolds of C_3O_2

parameter	units	ground state	ν_1 state[a]	ν_2 state	ν_3 state	ν_4 state
ν_0	cm^{-1}		2199.98	787.72	2289.80	1587.39
V_2	cm^{-1}/rad^2	−245	−243	−15	−431	−155
V_4	cm^{-1}/rad^4	698	667	633	725	665
V_B	cm^{-1}	21.5	22.1	0.1	65.3	49.3
θ_{min}	degrees	24.0	24.4	6.4	31.1	29.3

[a] Parameters for ν_1 from this work; other parameters from ref 20 and references therein.

because our ΔB value for ν_1 implies an increase of only 0.41 pm in the CO bond length (116.4 pm, ref 31) when ν_1 is excited (assuming R_{CC} is unchanged). In contrast, the changes in the potential are much larger when the ν_3 antisymmetric mode is excited, with V_B tripling to 65.3 cm^{-1} and θ_{min} increasing to 31.1°. In a similar way, the ν_4 antisymmetric excitation of the CC stretch leads to increases in V_B to 49.3 cm^{-1} and in θ_{min} to 29.3°. However, excitation of the ν_2 symmetric CC stretch almost eliminates the barrier, with $V_B = 0.1$ cm^{-1} and $\theta_{min} = 6.4°$; the bending potential in this case is almost purely quartic. These results suggest that symmetry of the charge flow during the course of the vibrations is an important factor in determining the ease with which bending can occur around the central carbon.

Axial Force Constants and Bonding in C_3O_2. Our value of ν_1, along with literature values for the ν_2, ν_3, and ν_4 axial modes, allows one to calculate some of the axial force constants for carbon suboxide. The relationships along with their calculated values are given in Tables3 and 4. There are six internal force constants describing axial motion but only four observables, so some assumptions are necessary. Because the CO units are well separated, it is reasonable to set the CO···CO interaction constant $f_{CO,CO}$ to zero. Assuming also that the CO···C′C

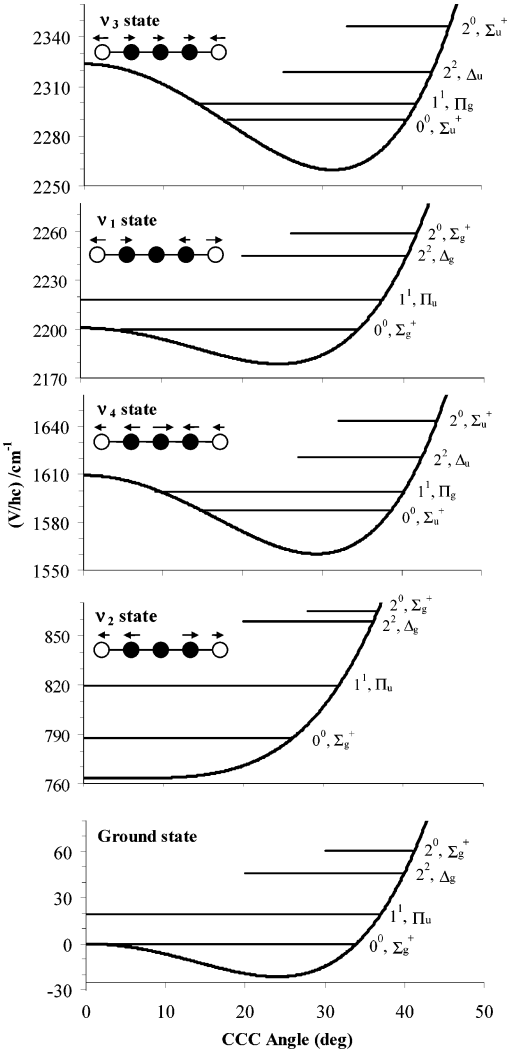

Figure 5. The effective ν_7 bending potentials for the ground and ν_1, ν_2, ν_3, and ν_4 vibrational states. The lowest levels of the ν_7 manifold are shown for each state.

TABLE 3: Axial Force Constant Relations for C_3O_2[a]

$$\lambda_1 + \lambda_2 = (\mu_O + \mu_C)F_{11} + \mu_C F_{22} - 2\mu_C F_{12}$$
$$\lambda_1\lambda_2 = \mu_O\mu_C(F_{11}F_{22} - F_{12}^2)$$
$$\lambda_3 + \lambda_4 = (\mu_O + \mu_C)F_{33} + 3\mu_C F_{44} - 2\mu_C F_{34}$$
$$\lambda_3\lambda_4 = (3\mu_O\mu_C + 2\mu_C^2)(F_{33}F_{44} - F_{34}^2)$$
$$F_{11} = f_{CO} + f_{CO,CO} \approx f_{CO}$$
$$F_{22} = f_{CC} + f_{CC,CC}$$
$$F_{12} = f_{CO,CC} + f_{CO,C'C} \approx f_{CO,CC}$$
$$F_{33} = f_{CO} - f_{CO,CO} \approx f_{CO}$$
$$F_{44} = f_{CC} - f_{CC,CC}$$
$$F_{34} = f_{CO,CC} - f_{CO,C'C} \approx f_{CO,CC}$$

[a] $\mu_i = m_i^{-1}$

interaction $f_{CO,C'C}$ is zero (because there is no shared C atom), we obtain result a in Table 4; if $f_{CO,C'C}$ is taken to be $^1/_4 f_{CO,CC}$, then result b is obtained. Also listed for comparison are some bond stretching force constants for a few other relevant molecules.

From these values, it can be seen that, in both cases a and b, the CO stretching constant falls between that of carbon monoxide (triple bond) and that of carbon dioxide (double bond). These results can be partially rationalized in terms of the valence bond resonance structures

$$\underset{\text{I}}{O{=}C{=}C{=}C{=}O} \leftrightarrow \underset{\text{II}}{{}^+O{\equiv}C{-}\bar{C}{=}C{=}O} \leftrightarrow \underset{\text{III}}{O{=}C{=}\bar{C}{-}C{\equiv}O^+}$$

TABLE 4: Internal Axial Force Constants (N/m) for C_3O_2 and Related Molecules

molecule		f_{CO}	f_{CC}	$f_{CC,CC}$	$f_{CO,CC}$
O=C=C=C=O	C_3O_2[a]	1654	1085	135	127
	C_3O_2[b]	1894	966	131	221
O=C=O	CO_2[c]	1550			
C≡O	CO[d]	1901			
C=C=C	C_3[e]		1026	45	
H_2C=C=CH_2	C_3H_4[f]		995	74	
H_2C=CH_2	C_2H_4[c]		957		

[a] This work, assuming $f_{CO,CO} = 0$ and $f_{CO,C'C} = 0$ [b] This work, assuming $f_{CO,CO} = 0$ and $f_{CO,C'C} = {}^1/_4 f_{CO,CC}$ [c] ref 33 [d] ref 34 [e] ref 35 [f] ref 36

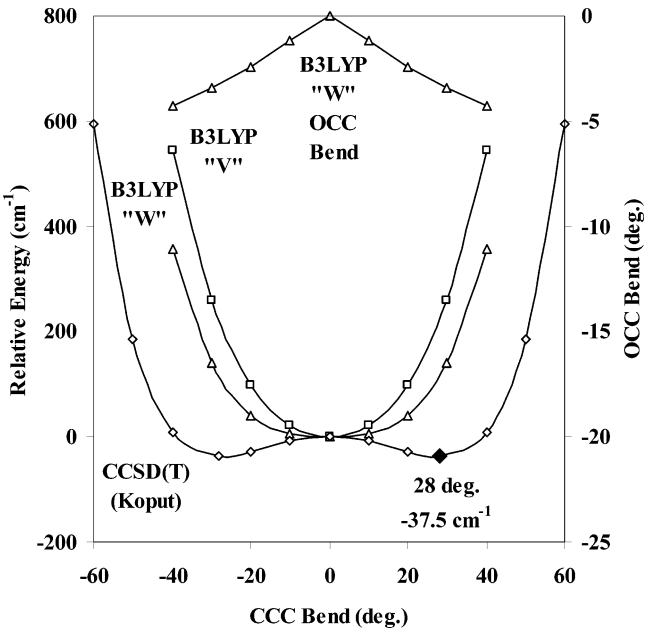

Figure 6. Effect of CCC bending on the energy and OCC angle for C_3O_2. See discussion in text.

Structure I, the classical representation, is generally thought to be mixed with ionic forms such as II and III. The latter ionic forms will tend to give somewhat stronger CO bonds, as observed, and also will favor bent structures, so that the low CCC bending frequency can be rationalized. However, the ionic forms would also predict a significant reduction in the C=C bond force constant, a result not actually seen in either case a or case b.

In 1974, Brown and Lipscomb[32] considered an alternative description of the bonding in terms of simple molecular orbitals, finding from calculations that the low bending frequency is favored when the HOMO orbitals take the shape of a three-centered bond over the central three C atoms. We have explored this further via Gaussian ab initio calculations[37] on C_3O_2 using density functional (B3LYP) methods with a large basis set, 6-311++g(3df,3pd). The calculations were done for various CCC bending angles and with the CCO angles fixed at 180° ("V" shape) or variable ("W" or trans CCCO shape). As seen in Figure 6, both calculations predict linear structures, but the potential is lower and flatter when the OCC angle is allowed to deviate a few degrees from 180°, as shown at the top of the figure. At the minimum, the CCC bending frequency is calculated as 30 cm^{-1}, about twice the experimental value of 18 cm^{-1}.

Displayed in Figure 7 are the changes in the orbital energies of the HOMO levels of C_3O_2 as the CCC angle is changed. For simple triatomic molecules, the variation in such levels has been

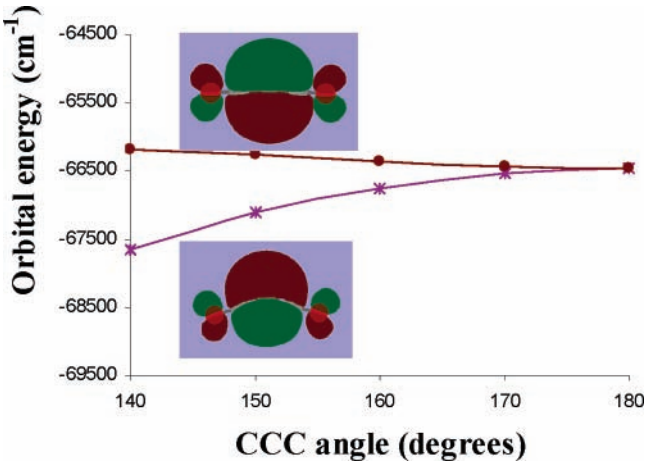

Figure 7. Effect of CCC bending on the HOMO orbital energy and shape for C_3O_2. The calculation is at the B3LYP level with a 6-311++g(3df,3pd) basis set.

used with some success in predicting the linearity or bent nature of the molecules (Walsh rules).[38] As seen in Figure 7, the highest HOMO orbital favors a linear geometry for C_3O_2, as does the total energy curve in Figure 6. However, these curves are quite flat, and the energy decrease with bending in the next lower orbital is consistent with the very low bending frequency in the molecule. Shown in Figure 7 for a CCC angle of 140° are the shapes for these two molecular orbitals, and it is seen that, as suggested by Brown and Lipscomb,[32] both are essentially three-centered combinations of the p orbitals on the three carbon atoms. The HOMO combination has the p orbitals perpendicular to the molecular plane, the next lower level has them in-plane, and interestingly, bending in this case causes a lowering of energy. At the linear geometry, these two levels have the same energy and shapes corresponding to orthogonal p_x or p_y three-centered orbitals.

Of course, the calculations at the B3LYP level do not reproduce the double minimum structural potential found from the spectroscopic data, but close correspondence is observed for higher-level calculations with large basis sets. Shown in Figure 6 are the recent ab initio results of Koput[12] from coupled cluster calculations (CCSD(T)/cc-pVQZ) that yield a double minimum potential with a maximum of 37.5 cm^{-1}, reasonably close to the experimental value of 24 cm^{-1}. Although this height was found to be somewhat sensitive to the method used to account for electron correlations, there is, in our view, a satisfying overall convergence of the experimental and ab initio results for this challenging "floppy" molecule.

Acknowledgment. We wish to thank Stéphanie Melin for assistance and helpful discussions in the early phases of this work. We acknowledge support by the National Science Foundation and Oregon State University for the CARS work and analysis performed at OSU.

References and Notes

(1) Diels, O.; Wolf, B. *Ber.* **1906**, *39*, 689.
(2) Shimizu, M. In *Proc.—Symp. Planet. Atmos.*; Jones, A. V., Ed.; Royal Society of Canada: Ottawa, 1977, p 67.
(3) Sheahen, T. P. *Combust. Flame* **1974**, *22*(2), 243.
(4) Plummer, W. T.; Carson, R. K. *Astrophys. J.* **1970**, *159*(1) Pt. 1, 159.
(5) Young, L.; Young, A. *Sci. Am.* **1975**, *233*(3), 71.
(6) Jenkins, E. B.; Morton, D. C. *Astrophys. J.* **1969**, *157*(2) Pt. 1, 913.
(7) Delitsky, M. L.; Lane, A. L. *J. Geophys. Res.* **1998**, *103*(E13), 31, 391.

(8) Huntress, W. T., Jr.; Allen, M.; Delitsky, M. *Nature (London)* **1991**, *352*, 316.
(9) Gerakines, P. A.; Moore, M. H. *Icarus* **2001**, *154*, 372.
(10) Oyama, V. I.; Berdahl, B. J.; Woeller, F. *Life Sci. Space Res.* **1979**, *17*, 47.
(11) Auwera, J. V.; Johns, J. W. C.; Polyansky, O. L. *J. Chem. Phys*. **1991**, *95*(4), 2299.
(12) Koput, J. *Chem. Phys. Lett*. **2000**, *320*(3, 4), 237.
(13) Gausset, L.; Herzberg, G.; Lagerqvist, A.; Rosen, B. *Astrophys. J*. **1965**, *142*(1), 45.
(14) Lolck, J.-E.; Brodersen, S. *J. Mol. Spec*. **1979**, *75*(2), 234.
(15) Lolck J.-E.; Brodersen, S.; *J. Mol. Spec*. **1978**, *72*(3), 445.
(16) Carreira, L. A.; Carter, R. O.; Durig, J. R.; Lord, R. C.; Milionis, C. C. *J. Chem. Phys.* **1973**, *59*(3) 1028.
(17) Walters, A. D.; Winnewisser, M.; Lattner, K.; Winnewisser, B. P. *J. Mol. Spec*. **1991**, *149*(2), 542.
(18) Weber, W. H.; Maker, P. D.; Peters, C. W. *J. Chem. Phys*. **1976,** *64*(5), 2149.
(19) Auwera, J. V.; Holland, J. K.; Jensen, P.; Johns, J. W. C. *J. Mol. Spec*. **1994**, *163*(2), 529.
(20) Fusina, L.; Mills, I. M. *J. Mol. Spec*. **1980**, *79*(1), 123.
(21) Jensen, P. *J. Mol. Spec*. **1984**, *104*(1), 59.
(22) Jensen, P.; Johns, J. W. C. *J. Mol. Spec*. **1986**, *118*(1), 248.
(23) Lafferty, W. J.; Maki, A. G.; Plyler, E. K. *J. Chem. Phys*. **1964,** *42*(1), 224.
(24) McDougall, L. E.; Kilpatrick, J. E. *J. Chem. Phys*. **1965**, *42*(7), 2311.
(25) *CRC Handbook of Chemistry and Physics*, 74th ed.; Lide, D., Ed.; CRC Press: Boca Raton, FL, 1993−1994. Stull, D. R. *Ind. Eng. Chem.* **1947**, *39*, 540.
(26) Leuchs, M.; Crew, M.; Harrison, J.; Hineman, M. F.; Nibler, J. W. *J. Chem. Phys*. **1996**, *105*, 4885.
(27) Gerstenkern, S.; Luc, P. *Atlas du Spectra d'Absorption de la Molecule d'Iode*; Centre National de la Recherche Scientifique: Paris, France, 1978.
(28) Vereschagin, K. A.; Smirnov, V. V.; Chrysostom, E. T. H.; Nibler, J. W. *J. Raman Spec*. **2000**, *31*(8/9), 719.
(29) Orlov, M. L.; Ogilvie, J. F.; Nibler, J. W. *J. Mol. Spec*. **1997**, *185*(1), 128.
(30) Duckett, J. A.; Robiette, A. G.; Mills, I. M. *J. Mol. Spec*. **1976**, *62*(1), 34.
(31) Walford, G.; Clarke, J. H.; Dore, J. C. *Mol. Phys.* **1978**, *36*(6), 1581.
(32) Brown, L. D.; Lipscomb, W. N. *J. Am. Chem. Soc*. **1977**, *99*(12), 3968.
(33) Herzberg, G. *Molecular Spectra and Molecular Structure: Infrared and Raman Spectra of Polyatomic Molecules*; Van Nostrand Co., Inc.: Princeton, NJ, 1945.
(34) Herzberg, G. *Spectra of Diatomic Molecules*; Van Nostrand Co., Inc.: Princeton, NJ, 1950.
(35) Ramaswamy, K.; Balasubramanian, V. *Indian J. Pure Appl. Phys*. **1972**, *10*(12), 853.
(36) Venkateswarlu, K.; Pillai, M. G.; Krishna *Z. Physik. Chem*. **1958**, *18*, 396.
(37) Frisch, M. J.; Trucks, G. W.; Schlegel, H. B.; Scuseria, G. E.; Robb, M. A.; Cheeseman, J. R.; Montgomery, J. A., Jr.; Vreven, T.; Kudin, K. N.; Burant, J. C.; Millam, J. M.; Iyengar, S. S.; Tomasi, J.; Barone, V.; Mennucci, B.; Cossi, M.; Scalmani, G.; Rega, N.; Petersson, G. A.; Nakatsuji, H.; Hada, M.; Ehara, M.; Toyota, K.; Fukuda, R.; Hasegawa, J.; Ishida, M.; Nakajima, T.; Honda, Y.; Kitao, O.; Nakai, H.; Klene, M.; Li, X.; Knox, J. E.; Hratchian, H. P.; Cross, J. B.; Adamo, C.; Jaramillo, J.; Gomperts, R.; Stratmann, R. E.; Yazyev, O.; Austin, A. J.; Cammi, R.; Pomelli, C.; Ochterski, J. W.; Ayala, P. Y.; Morokuma, K.; Voth, G. A.; Salvador, P.; Dannenberg, J. J.; Zakrzewski, V. G.; Dapprich, S.; Daniels, A. D.; Strain, M. C.; Farkas, O.; Malick, D. K.; Rabuck, A. D.; Raghavachari, K.; Foresman, J. B.; Ortiz, J. V.; Cui, Q.; Baboul, A. G.; Clifford, S.; Cioslowski, J.; Stefanov, B. B.; Liu, G.; Liashenko, A.; Piskorz, P.; Komaromi, I.; Martin, R. L.; Fox, D. J.; Keith, T.; Al-Laham, M. A.; Peng, C. Y.; Nanayakkara, A.; Challacombe, M.; Gill, P. M. W.; Johnson, B.; Chen, W.; Wong, M. W.; Gonzalez, C.; Pople, J. A. *Gaussian 03*, revision B.05; Gaussian, Inc.: Pittsburgh, PA, 2003.
(38) Walsh, A. D. *J. Chem. Soc.* **1953**, 2260.